Accepted Manuscript

Eco-friendly preparation of electrically conductive chitosan - reduced graphene oxide flexible bionanocomposites for food packaging and biological applications

Ana Barra, Nuno M. Ferreira, Manuel A. Martins, Oana Lazar, Aida Pantazi, Alin Alexandru Jderu, Sabine M. Neumayer, Brian J. Rodriguez, Marius Enăchescu, Paula Ferreira, Cláudia Nunes

PII: S0266-3538(18)32838-0

DOI: https://doi.org/10.1016/j.compscitech.2019.01.027

Reference: CSTE 7549

To appear in: *Composites Science and Technology*

Received Date: 21 November 2018

Revised Date: 22 January 2019

Accepted Date: 25 January 2019

Please cite this article as: Barra A, Ferreira NM, Martins MA, Lazar O, Pantazi A, Jderu AA, Neumayer SM, Rodriguez BJ, Enăchescu M, Ferreira P, Nunes Clá, Eco-friendly preparation of electrically conductive chitosan - reduced graphene oxide flexible bionanocomposites for food packaging and biological applications, *Composites Science and Technology* (2019), doi: https://doi.org/10.1016/j.compscitech.2019.01.027.

Eco-friendly preparation of electrically conductive chitosan - reduced graphene oxide flexible bionanocomposites for food packaging and biological applications

Ana Barra[a], Nuno M. Ferreira[a,b], Manuel A. Martins[a], Oana Lazar[c], Aida Pantazi[c], Alin Alexandru Jderu[c], Sabine M. Neumayer[d,e], Brian J. Rodriguez[d], Marius Enăchescu[c,f], Paula Ferreira[a*], Cláudia Nunes[a*]

[a]CICECO - Aveiro Institute of Materials, Department of Materials and Ceramic Engineering, University of Aveiro, 3810-193 Aveiro, Portugal

[b]I3N, Department of Physics, University of Aveiro, 3810-193 Aveiro, Portugal

[c]Center for Surface Science and NanoTechnology, University Polytechnic of Bucharest, Romania

[d]School of Physics & Conway Institute of Biomolecular and Biomedical Research, University College Dublin, Belfield, Dublin 4, Ireland

[e]Center for Nanophase Materials Sciences, Oak Ridge National Laboratory, 1 Bethel Valley Rd. Oak Ridge, TN 37831, USA

[f]Academy of Romanian Scientists, Bucharest, Romania

Corresponding Authors:

Cláudia Nunes: e-mail: claudianunes@ua.pt; phone: +351 234370706; fax: +351 234401470

Paula Ferreira: e-mail: pcferreira@ua.pt; phone: +351 234401419; fax: +351 234401470

Abstract

Electrically conductive materials have been highlighted in the biomedical and food packaging areas. Conventional electrically conductive polymers have limited biodegradability and biocompatibility and should be replaced by suitable biomaterials. Herein, electrically conductive bionanocomposites of chitosan and reduced graphene oxide were produced by a green methodology. The reduced graphene oxide was hydrothermally reduced in the presence of caffeic acid and was dispersed into chitosan. The final bionanocomposites achieved an electrical conductivity of 0.7 S/m in-plane and 2.1×10^{-5} S/m through-plane. The reduced graphene oxide promoted a great enhancement of antioxidant activity and a mechanical reinforcement of chitosan matrix, increasing the tensile strength and decreasing the water solubility. The electrical conductivity, mechanical properties and antioxidant activity of the bionanocomposites can be tuned according to the filler content. These active bionanocomposites, prepared using a green methodology, revealed good electrical and mechanical properties, which make them promising materials for food packaging and biological applications.

Keywords: bionanocomposites, chitosan, reduced graphene oxide, hydrothermal reduction, electrical conductivity

1. Introduction

Electrically conductive biomaterials are promising for applications at the interface between biology and electronics, being employed in biomedical scaffolds, sensors and actuators, as well as electrically conductive food packaging [1–4]. Electrically conductive polymers can be used to provide the necessary electrical conductivity, but their cytotoxicity and the lack of biocompatibility and biodegradability prevents their use for food and biological applications. Thus, the development of biocomposites using nontoxic electrically conductive fillers and natural biopolymers with bioactivity can overcome this problem [5].

Chitosan (CS) is an abundant and renewable biopolymer, with a great film forming ability, biodegradability and nontoxicity. This biopolymer has been actively investigated for food packaging and biomedical applications due to its antimicrobial and antioxidant activity, which are important properties to extend the shelf life of food and prevent inflammatory responses [6–10]. However, it is necessary to improve the poor electrical and mechanical properties of CS through its combination with appropriate electrically conductive fillers [11,12].

Reduced graphene oxide (rGO), is an electrically conductive graphene-based material with high mechanical performance and biocompatibility [13,14]. The use of rGO in materials for biomedical and food packaging applications as well as its effectiveness to reinforce the mechanical, gas and water barrier, and electrical properties of biopolymers have been reported by several authors [15–18]. rGO is commonly synthesized through the chemical oxidation of graphite by the Hummers method producing graphene oxide (GO), followed by a reduction step to restore the graphitic network. This methodology preserves some oxygen containing groups to establish chemical interactions with the positively

charged amine groups of CS and reinforce the composites [11,19,20]. The synthesis of rGO for biomedical and food applications must avoid toxic reducing agents. Therefore, it should consider green reduction strategies, as thermal reduction or chemical reduction processes that can combine the use of non-toxic compounds and mild temperatures [21].

Several non-toxic compounds have been reported to reduce GO [22]. Zhou T. *et al.* [23], reduced GO using a solution of sodium hydrosulfite and sodium hydroxide at 60 °C during 15 minutes, achieving an electrical conductivity of 1377 S/m. In addition, CS biopolymer was also used as a biocompatible reducing agent to prepare a drug delivery system at low temperature (37 °C) during 72 h [24]. Diverse vitamins and phenolic compounds were explored as natural reducing agents, namely L-ascorbic, vitamin C, and green tea polyphenolic extract [25–27][28]. Bo *et al.* [27] reported the use of caffeic acid (3,4-dihydroxycinnamic acid), a phenolic compound naturally present in plants with high antioxidant activity [29], as an effective green reducing agent able to produce rGO with a high C/O ratio (7.15). Besides that, the use of caffeic acid can not only reduce GO but also impart antioxidant activity to the materials prepared with rGO. The preparation of CS grafted caffeic acid active films with enhanced antioxidant activity was reported by our group [30]. The efficiency of these reduction methods can be complemented with thermal treatments to improve the electrical conductivity of rGO. Kim *et al.* [31] reported the synthesis of rGO using dextran as reducing agent with an electrical conductivity of 1.1 $S \cdot m^{-1}$ and its increment to 10000 $S \cdot m^{-1}$ after annealing rGO papers at 500 °C during 2 h under argon atmosphere. The hydrothermal treatment of GO is also an environmentally friendly and scalable methodology to reduce GO. This methodology produces rGO with high electrical conductivity and mechanical strength. The high pressure and temperature generated inside the autoclave removes the oxygen containing groups from GO converting

them into CO_2, CO and low molecular weight organic fragments. Therefore, this water-based methodology produces rGO with improved electrical conductivity [32,33].

The main aim of this study is the development of an electrically conductive bionanocomposite using CS, a bioactive polymer, and rGO. GO was prepared by an improved Hummers method and was further hydrothermally reduced in the presence of caffeic acid, a non-toxic compound. The bionanocomposites were prepared with different amounts of rGO and the films structure, morphology, mechanical, electrical and antioxidant properties were characterized to evaluate their potential for food packaging and biological applications.

2. Experimental

2.1 Materials

Chitosan (medium molecular weight, 75-85% deacetylated), glacial acetic acid (99,8%), graphite flakes (~150 μm), phosphoric acid (≥85%), sulfuric acid (97%), potassium permanganate (99,0%), hydrochloric acid (37%), hydrogen peroxide (30%) and caffeic acid (≥95%) were purchased from Sigma-Aldrich Co. (St Louis, MO, USA) and used as received. Glycerol (95%) was purchased from Scharlab, S.L. (Barcelona, Spain). All other reagents used were of analytical grade.

2.2 Preparation of bionanocomposite films

2.2.1 Synthesis of GO

GO was synthesized by an improved Hummers method [19]. Graphite flakes (0.75 g) were added to phosphoric and sulphuric acid (1:9), previously to the slow addition of

potassium permanganate (4.5 g). The mixture remained under stirring at 50 °C overnight and after being cooled down to the room temperature, ice (50 mL) and hydrogen peroxide 10% (2.5 mL) were added. The final product was centrifuged (4000 rpm, 30 min at room temperature) and the precipitate washed with distilled water (100 mL), hydrochloric acid 30% (100 mL) and ethanol (2 x 100 mL). GO was dispersed into distilled water with an ultrasonic homogenizer (SONOPULS HD 3100, 45W, 1 h) and stored for future use.

2.2.2 Reduction of GO

GO was hydrothermally reduced in the presence of caffeic acid. Equal amounts of GO and caffeic acid were dispersed in distilled water in a teflon lined autoclave and placed in the oven for 24 h at 180 °C. After cooling down the autoclave to the room temperature, the obtained rGO was filtered with filter paper (Filter-Lab 1300/80) and washed several times with distilled water.

2.2.3 Films preparation

Several amounts of rGO (0, 25, 40, 45, 48 or 50 wt%, in relation to CS weight) were dispersed in distilled water using the ultrasonic homogenizer at 45 W during 20 min. Acetic acid solution (0.1 M) and CS (1.5%, w/v) were added to the rGO dispersions and remained under stirring overnight for complete dissolution of CS. Glycerol 0.75% (m/v) was used as plasticizer and homogenized by stirring during 10 min at 50 °C, followed by the solutions filtration with a nylon mesh cloth. To prepare the films by solvent casting, the CS-rGO solutions (31 g) were distributed in acrylic plates (144 cm^2) and dried overnight at 35 °C inside an air circulating oven. The bionanocomposites films will be mentioned according to its rGO load: CS-rGO25 (25%), CS-rGO40 (40%), CS-rGO45 (45%), CS-rGO48 (48%), and CS-rGO50 (50%). The control sample CS/glycerol blend (0% rGO) will be further mentioned as CS.

137

138 **2.3 Characterization of bionanocomposite films**

139 **2.3.1 Structural and morphological characterization**

140 **X-Ray Diffraction (XRD)** analysis was carried out on a SmartLab (Rigaku) X-Ray
141 Diffractometer. The high-resolution XRD patterns were recorded at 9 kW (45 kV and 200
142 mA) with Cu target K_α radiation (λ=0.15406 nm) passing through a Ni-filter. The films
143 from this study were investigated in Parallel Beam Geometry, in a continuous mode scan, at
144 a step size of 0.01^o and scanning speed of 10 ^{o}/min, while the powder sample (rGO) was
145 analyzed in Bragg Brentano Geometry (continuous mode) with a 0.01^o step size and
146 scanning speed of 3 ^{o}/min.

147 **Raman spectroscopy** was conducted at room temperature by confocal micro-Raman
148 Spectroscopy, using a LabRam HR800 (Horiba) system. All Raman spectra were generated
149 by exposing the samples to a 532/632 nm wavelength green/red excitation laser.

150 **Scanning electron microscopy (SEM)** and **Scanning transmission electron microscopy**
151 **(STEM)** were performed using a SU-8230 (Hitachi) SEM microscope at an accelerating
152 voltage of 10 kV and a HD-2700 (Hitachi) STEM microscope with an accelerating voltage
153 of 200 kV. For STEM, the films were prepared via ultramicrotomy and deposited on
154 standard Cu TEM grids with formvar and lacey carbon polymeric films.

155 **Atomic force microscopy (AFM)** and **conductive atomic force microscopy (C-AFM)**
156 were carried out in an MFP-3D AFM microscope (Asylum Research) in intermittent
157 contact mode. DPE18 Pt-coated cantilevers (MikroMasch) with nominal resonance
158 frequencies of 75 kHz and spring constants of 3.5 N/m, were used for AFM analysis. HQ:
159 DPE-XSC11 Pt-coated cantilevers (MikroMasch), with resonance frequency of 80 kHz and
160 spring constants of 2.7 N/m were used for C-AFM analysis.

2.3.2 Physical and biological characterization

Electrical conductivity of the bionanocomposite films was determined at room temperature by direct current (*dc*) measurements. The electrical response in-plane was determined using samples with 0.5 x 3.5 cm and a home-made 4-point probe resistivity setup. The electrical response through-plane was determined using 1 cm^2 square samples in a home-made 2-point probe resistivity setup [34]. For these measurements a programmable power supply IPS603 (ISO-Tech) and two 34401A Multimeters (HP) were used. The calculations were made using Equation 1.

$$R = \frac{V}{I} = \rho \frac{l}{A} = \frac{1}{\sigma} \frac{l}{A} \qquad \text{Equation 1}$$

where the parameters are the conventional denomination in electrical circuits: resistance (R), tension (V), current (I), resistivity (ρ), and electrical conductivity (σ). The definition of *l* and *A* is dependent of the measurement setup. The electrical conductivity was measured in triplicate.

Tensile tests until film rupture were carried out according to the standard method (ASTM D 882-83) on a TA HDi texture analyzer equipment (Stable Micro Systems) using a 5 Kg load cell. The films were cut into 6 stripes of 90 x 10 mm and their thickness was measured with a digital micrometer (Mitutoyo Corporation) with approximately 0.001 mm accuracy. The films were kept into a moisture and temperature controlled chamber (RH 45%; 22 °C) during 5 days prior to analysis. Six stripes of each bionanocomposite were tested.

Water contact angle between an ultra-pure water drop (3 µL) and the bionanocomposites was measured using an OCA contact angle system (Dataphysics) by the Laplace - Young method. The films were kept into a moisture- and temperature-controlled chamber (RH

45%; 22 °C) for 2 days prior to analysis. Ten contact angle values were determined for each sample.

Moisture (M) and solubility (S) of bionanocomposites were determined by averaging the weight loss percentage of at least 6 samples [30]. The films were weighted (mi), dried overnight in an oven at 105 °C and reweighted (mf). The moisture was determined using Equation 2.

$$M(\%) = \frac{mi-mf}{mi} \times 100\% \quad \text{Equation 2}$$

To determine the solubility in acidic conditions, 4 cm^2 film samples were weighted (initial mass), immersed into 30 mL of water acidified with hydrochloric acid (pH 3.5) and placed in an orbital stirrer at 80 rpm. After 7 days, the samples were dried overnight in an oven at 105 °C and reweighted (final mass) The initial and final film mass were corrected considering the films moisture. The solubility was calculated using Equation 3.

$$S(\%) = \left(\frac{Initial\ mass - Final\ mass}{Inicial\ mass}\right) \times 100\% \quad \text{Equation 3}$$

Three samples of each bionanocomposite were analyzed.

Antioxidant activity of bionanocomposites was assessed by the 2,2′-azinobis-(3-ethyl-benzothiazoline-6-sulfonic acid) ($ABTS^{\bullet+}$) decolorization assay [35]. 1 cm^2 film samples were immersed in an $ABTS^{\bullet+}$ solution (diluted 1:80 in ethanol) and placed in an orbital stirrer at 80 rpm. After 8 h, the absorbance (abs) of the $ABTS^{\bullet+}$ solution without film (control) and the $ABTS^{\bullet+}$ solutions with films were measured. The antioxidant activity was calculated by means of $ABTS^{\bullet+}$ inhibition by the films applying Equation 4.

$$Inhibition\ (\%) = \left(\frac{abs\ control - abs\ film}{abs\ control}\right) \times 100\% \quad \text{Equation 4.}$$

The antioxidant activity of the bionanocomposites was analyzed in triplicate.

2.4 Statistical analysis

The results of electrical conductivity, mechanical properties, solubility, antioxidant activity and contact angle were statistically analyzed through one-way ANOVA with post-hoc Tukey tests, using a significance level of $p<0.05$. The data was analyzed using Origin 8.6 software.

3. Results and discussion

3.1 Structural evaluation by XRD and Raman spectroscopy

The crystalline structure of initial materials, GO, rGO and CS, as well as of bionanocomposites with the lowest and highest content of rGO, CS-rGO25 and CS-rGO50, was investigated by XRD (Fig. 1). The GO diffraction pattern shows a strong peak at 2θ = 10.4°, corresponding to the reflection (001). After the reduction, the rGO diffractogram presents a new peak at 2θ = 25.7°, corresponding to the (002) reflection, and a smooth peak at ~ 10°. This difference in spectra corroborates the occurrence of the reduction process, as well as the presence of remaining GO. The GO peak at 2θ = 10.4° corresponds to an interlayer spacing between sheets of 8.5 Å, while the peak that appears after reduction corresponds to a smaller d-spacing of 3.45 Å. This decrease of the d-spacing value after reduction is due to the elimination of oxygen content between sheets during the reduction of GO [19,36–38]. CS is a semi-crystalline biopolymer and shows a broad peak at 2θ = 21.1°, which can be assigned to the (110) reflection [39]. The above-mentioned signature peaks of CS and rGO are preserved in both bionanocomposites diffractograms. The CS-rGO25 bionanocomposite keeps the intense peak of CS and shows a very weak peak of rGO due to higher CS content (75%, w/w). Accordingly, CS-rGO50 shows both rGO and CS peaks with similar intensity due to the equal CS and rGO loads. The preservation of both CS and rGO peaks indicates a good homogenization

between the filler and matrix phase. The *d*-spacing of rGO peak at ~25° did not change significantly with its incorporation into CS. This result suggests that CS chains should not be intercalated into the rGO sheets, which is in good agreement with the typical self-folded rGO morphology resultant from the hydrothermal reduction process [40].

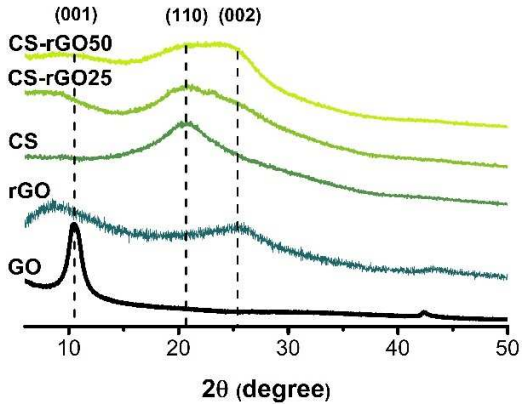

Fig. 1. XRD diffraction patterns of GO, rGO, CS, and bionanocomposites CS-rGO25 and CS-rGO50.

The structure of rGO and its alterations after the incorporation in CS matrix were evaluated by Raman spectroscopy (Fig. 2). The Raman spectra of both GO and rGO presents the characteristic graphitic D, G, and 2D bands. The D band, also known as the disorder band at ~1345 cm^{-1}, corresponds to the breathing modes of sp^2 rings and requires the proximity to a defect to be active. The G band at ~1589 cm^{-1} is attributed to the in-plane vibrational modes of sp^2 hybridized carbon atoms [41]. The I_D/I_G ratio is similar after the reduction process, 1.04 for GO and 1.06 for rGO, mainly due to the slight decrease of D band intensity. During the reduction of GO, new sp^2 domains are formed, but they exhibit a smaller average size in comparison with the previous existing sp^2 domains on GO, which

lead to a decreased G band intensity [42]. The 2D band at 2721 cm^{-1} is the second order D band and is active independently of the presence of a defect. The 2D band splits into the D+G at 2919 cm^{-1} and 2D' at 3136 cm^{-1}. The split of 2D band suggests a multilayer graphene sample [43]. The CS-rGO25 and CS-rGO50 bionanocomposites display a similar spectrum to rGO, which is an indication of a good rGO dispersion in the CS matrix with the preservation of its structure. The I_D/I_G increase observed after the rGO incorporation into the CS matrix (1.22 for CS-rGO25 and 1.26 for CS-rGO50), can be attributed to an increment of defects/edges in rGO due to blending with CS.

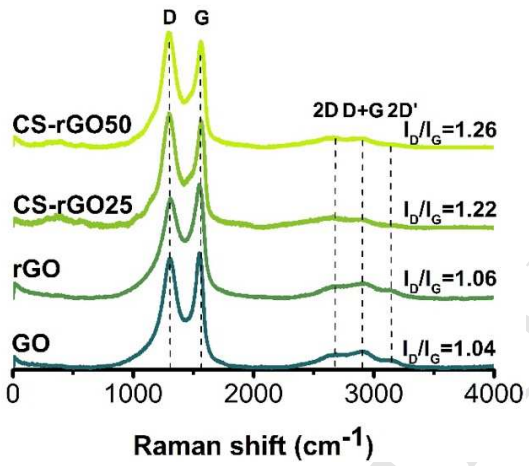

Fig. 2. Raman spectra of GO, rGO, and bionanocomposites CS-rGO25 and CS-rGO50, with the corresponding I_D/I_G values marked.

3.2 Morphological evaluation by SEM and STEM

The morphology of CS, CS-rGO25, and CS-rGO50 films was observed by SEM and STEM (Fig. 3). The chitosan film with the glycerol as plasticizer has a smooth surface that becomes wrinkled with the incorporation of rGO. The bionanocomposites SEM images present folded rGO sheets with a layered assembly due to the hydrothermal synthesis of rGO [44,45]. The CS-rGO50 cross-section shows a predominant organization of rGO

sheets in parallel to film thickness. Moreover, from the SEM images it is observed a good distribution of rGO through all the CS matrix. However, the STEM images of both bionanocomposites reveal rGO agglomerates wrapped by CS. This morphological analysis allows to conclude that rGO in the form of agglomerates are well distributed along the biocomposite.

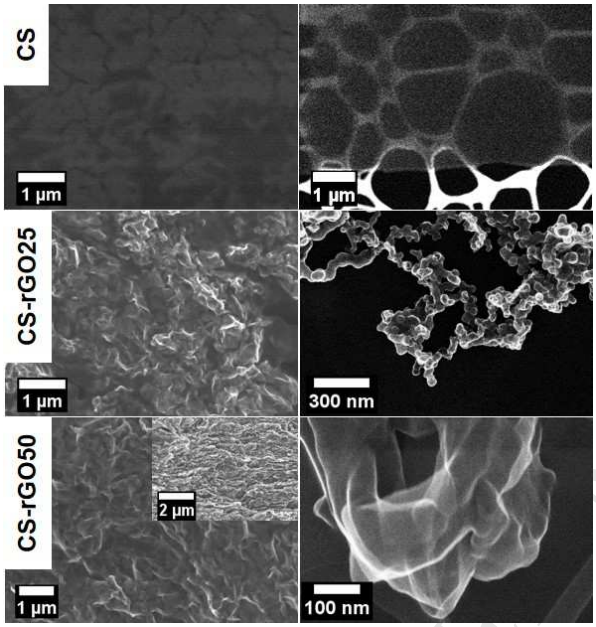

Fig. 3. SEM and STEM images. SEM images of CS and bionanocomposites (CS-rGO25 and CS-rGO50) films, with CS-rGO50 cross-section inset are displayed on the left column, while STEM images of CS and the bionanocomposites CS-rGO25 and CS-rGO50 are displayed on the right column.

3.3 Mechanical properties, solubility and wettability

The mechanical parameters like tensile strength (TS), Young's modulus (YM) and elongation at break (E), of CS and bionanocomposites were measured by tensile tests until rupture using several stripes of films (at least 6) to insure representative results of all film

(Fig. 4). The chitosan/glycerol film (CS) present mechanical properties (TS, YM, and E values) similar to those reported in the literature for chitosan films with addition of glycerol as plasticizer [46,47], while the TS and YM are lower and the E higher in relation to chitosan films without plasticizer [48,49]. The incorporation of 50% of rGO improves 2 times the TS from 13 MPa to 27 MPa and the YM is increased almost 6 times, from 0.47 GPa to 2.73 GPa, while the elongation decreased 10 times. The increase of both TS and YM, and the decrease of E, meaning an increase in resistance and a flexibility decrease, is a trend of CS-rGO composites well described in the literature [26,50–52]. Table S1 presents the mechanical parameters of CS-rGO composites reported in literature. To the best of author's knowledge, the improvement of resistance to the tension of this work is the best result achieved using rGO reduced by a green methodology. The improvement of TS is due to the reinforcing effect of rGO since no grafting strategies or other reinforcing components were used. The reinforcing effect of CS by rGO is well known, but it is reported that the use of high concentrations of rGO promotes its agglomeration and causes a decrease of TS and YM [11,50]. However, this study shows the use of rGO 50% enhance these parameters, which indicates that rGO is well dispersed into the CS matrix, allowing an efficient load transfer between both phases.

The solubility of CS and bionanocomposite films was determined by immersing the films in acidic aqueous medium (pH 3.5) for 7 days (Fig. 4). The CS solubility is approximately 34% and should be mainly due to glycerol diffusion to the water, as reported before for chitosan-based films [53]. The CS-rGO25 bionanocomposite shows a solubility of 30%, while the bionanocomposites with 40 – 48% of rGO load show a solubility of 24% and the CS-rGO50 has a solubility of 29%. This lower solubility could not be attributed to the lower content of CS in the films with the higher percentage of rGO, since the

305 percentage of solubility decrease is not proportional to the increase of rGO and the CS-
306 rGO50 showed a higher solubility than 40 – 48% of rGO films. These results indicate that
307 rGO reinforces water resistance of the films.

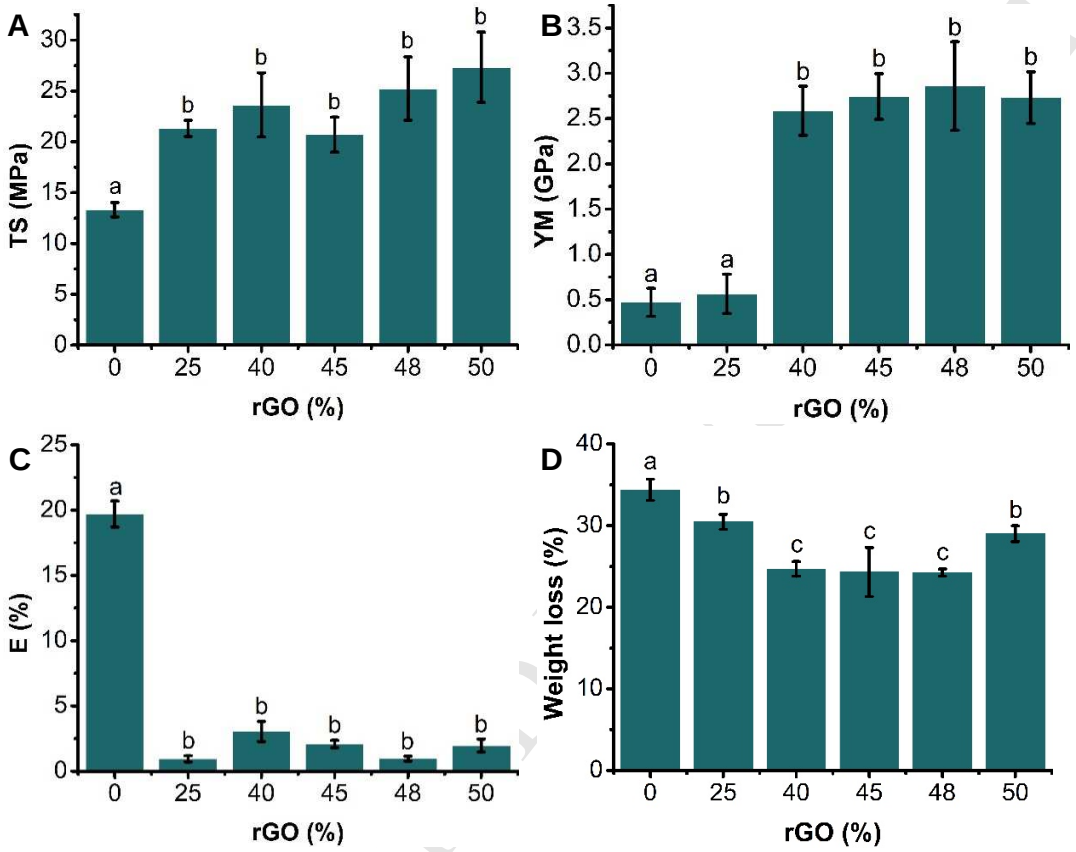

308

309 Fig. 4. Mechanical properties of CS and bionanocomposites CS-rGO25, CS-rGO40, CS-
310 rGO45, CS-rGO48 and CS-rGO50. (**A**) Tensile strength (TS), (**B**) Young's modulus (YM),
311 (**C**) elongation (E) and (**D**) water solubility (weight loss%). Different letters represent
312 significant ($p<0.05$) values (n=3).

313

314 The wettability of the films surface was investigated by water contact angle
315 measurements (Fig. 5). CS showed a water contact angle of 107°, inferring a hydrophobic
316 character of the films surface. This result is in good agreement with the values previously

reported for chitosan [46,54] and chitosan/glycerol films [30,47]. Chitosan is usually reported to be hydrophilic with a lower water contact angle [55]. However, CS were produced by solvent casting, which enhance the interaction between the hydrophilic groups, as well as the presence of glycerol that establish bonds with the amine and hydroxyl groups of the chitosan, reducing the interaction of these groups with water and increasing the surface hydrophobicity of the films. As described in the literature, the chitosan films have initial contact angles around 100°, but after few seconds there is a decrease of the contact angle that is related with the water absorption capacity or to capillary forces in the film–water interface due to the hydrophilic character of chitosan [56].

The rGO is hydrophobic due to the removal of oxygen containing groups [57]. However, the bionanocomposites show low contact angle values, between 68 – 77°. The increase of hydrophilicity can be explained due to the electrostatic and hydrogen bonding between CS amine groups and the remaining oxygen containing groups of rGO [58]. These interactions can lead to a higher exposition of CS hydroxyl groups at bionanocomposites surface and thus their interaction with water causes the decrease of contact angle values. Moreover, the incorporation of rGO increased the films roughness, which is associated with an enhancement of hydrophilicity [59].

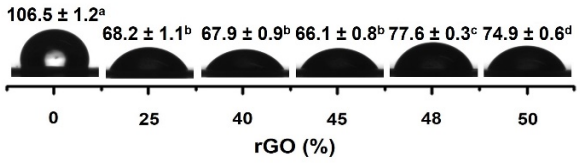

Fig. 5. Water contact angle value of CS film and bionanocomposites CS-rGO25, CS-rGO40, CS-rGO45, CS-rGO48, and CS-rGO50. Different letters represent significant (p<0.05) values (n=6).

3.4 Antioxidant activity

The antioxidant activity of CS and all the bionanocomposites was evaluated by the $ABTS^{\bullet+}$ inhibition method (Fig. 6). The incorporation of rGO into CS matrix lead to a great enhancement of antioxidant activity. After 8 hours of incubation, CS showed an $ABTS^{\bullet+}$ inhibition of 1%, while the bionanocomposite films showed an increase of inhibition with filler content in the range of 54% - 82%. The antioxidant activity can be attributed to the radical scavenging capacity of rGO [60]. Moreover, the presence of remaining caffeic acid, can also contribute to improve the antioxidant activity. In a similar work reported by our group, where CS was grafted with caffeic acid, films were achieved with an antioxidant activity 80% higher [30].

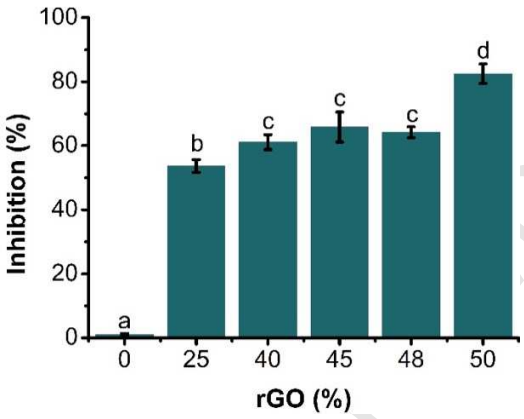

Fig. 6. Antioxidant activity (inhibition %) after 8 hours of incubation in $ABTS^{\bullet+}$ solution of CS and bionanocomposites CS-rGO25, CS-rGO40, CS-rGO45, CS-rGO48, and CS-rGO50. Different letters represent significant (p<0.05) values (n=3).

3.5 Electrical properties

The electrical conductivity of CS film and all the bionanocomposites was measured at macroscale by *dc* measurements in-plane and through-plane (Fig. 7). The electrical

conductivity increases with filler content above 45% of rGO (CS-rGO45) and 25% of rGO (CS-rGO25) for in-plane and through-plane conductivity, respectively. The maximum in-plane conductivity is 0.7 S/m with 50% of rGO (CS-rGO50), while the maximum through-plane conductivity is achieved with 45% of rGO ($2.1x10^{-5}$ S/m). The electrical conductivity in-plane is around 4 orders of magnitude greater than it is through-plane, which is explained by the preferential alignment of rGO along the plane direction [61]. The increment of electrical conductivity with the incorporation of rGO into the insulating CS matrix proves the efficiency of the GO hydrothermal reduction in presence of caffeic acid.

Table S1 presents the in-plane electrical properties of CS-rGO composites reported in the literature. The use of chemical compounds as nitrenes [51], hydrazine [52], and hydroiodic acid [62], as reducing agents is a good strategy to produce rGO with high electrical conductivity, due to the effectiveness of the reduction process. However, the toxicity of these chemical compounds prevents the use of rGO and its composites for biological applications. The use of alternative eco-friendly methodologies to reduce GO and prepare CS-rGO is reported in literature. For example, the use of tea polyphenol solution at 90 °C under nitrogen atmosphere, achieved an electrical conductivity of ~ 0.01 S/m with 1% rGO [50]. The *in situ* reduction of GO by CS (37 °C for 72 h) produced bionanocomposites with a slight higher electrical conductivity of 0.06 S/m, but using 7% rGO [50]. The immersion of CS-GO films containing 10% of GO in NaOH and $Na_2S_2O_4$ solutions at 60°C, originated films with an identical electrical conductivity (0.1 S/m) [11]. Therefore, this works reports the CS-rGO bionanocomposite with the highest in-plane electrical conductivity (0.7 S/m) prepared with 50% of rGO reduced by a green methodology.

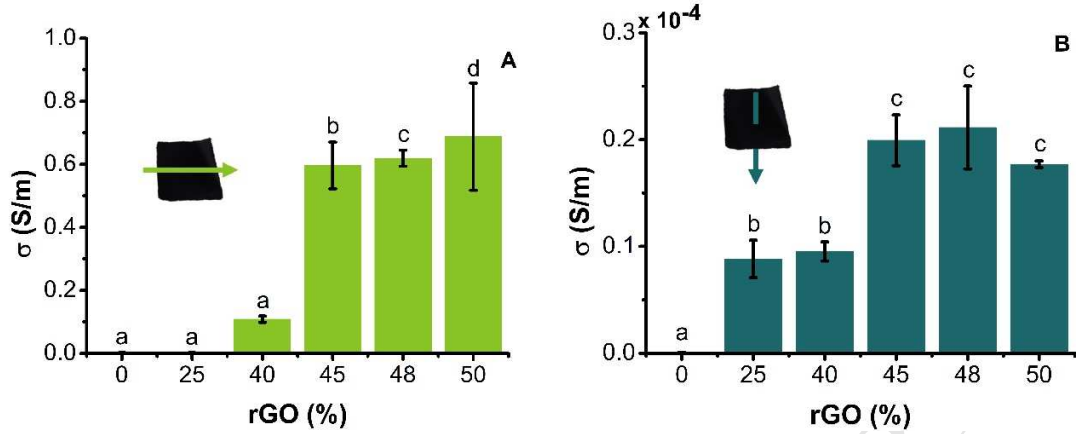

Fig. 7. Electrical conductivity of CS and bionanocomposites CSGO25, CS-rGO40, CS-rGO45, CS-rGO48, and CS-rGO50:(**A**) in-plane and (**B**) through-plane. Different letters represent significant (p<0.05) values (n=3).

The insulator CS, the low conductive CS-rGO40 and the high conductive CS-rGO50 samples were characterized by CAFM, with simultaneous acquisition of AFM images, to correlate the origin of the electrical conductivity with the topographic characteristics (Fig. 7). The AFM analysis shows the flat surface of the CS film becomes rough with the increment of rGO, which is in good agreement with the enhancement of the films wettability. The root mean square (RMS) roughness determined by AFM in a scan area of 5 µm x 5 µm also reveals an increment of surface roughness, from 0.6 nm on the CS film to 25 nm on CS-rGO40 and to 165 nm on CS-rGO50. Similarly, the CS film exhibits an insulating surface that becomes slightly conductive in CS-rGO40 and widely conductive in the CS-rGO50. The correlation between topography and electrical conductivity at the nanoscale is well established since the origin of surface roughness and current can be easily identified from the rGO location.

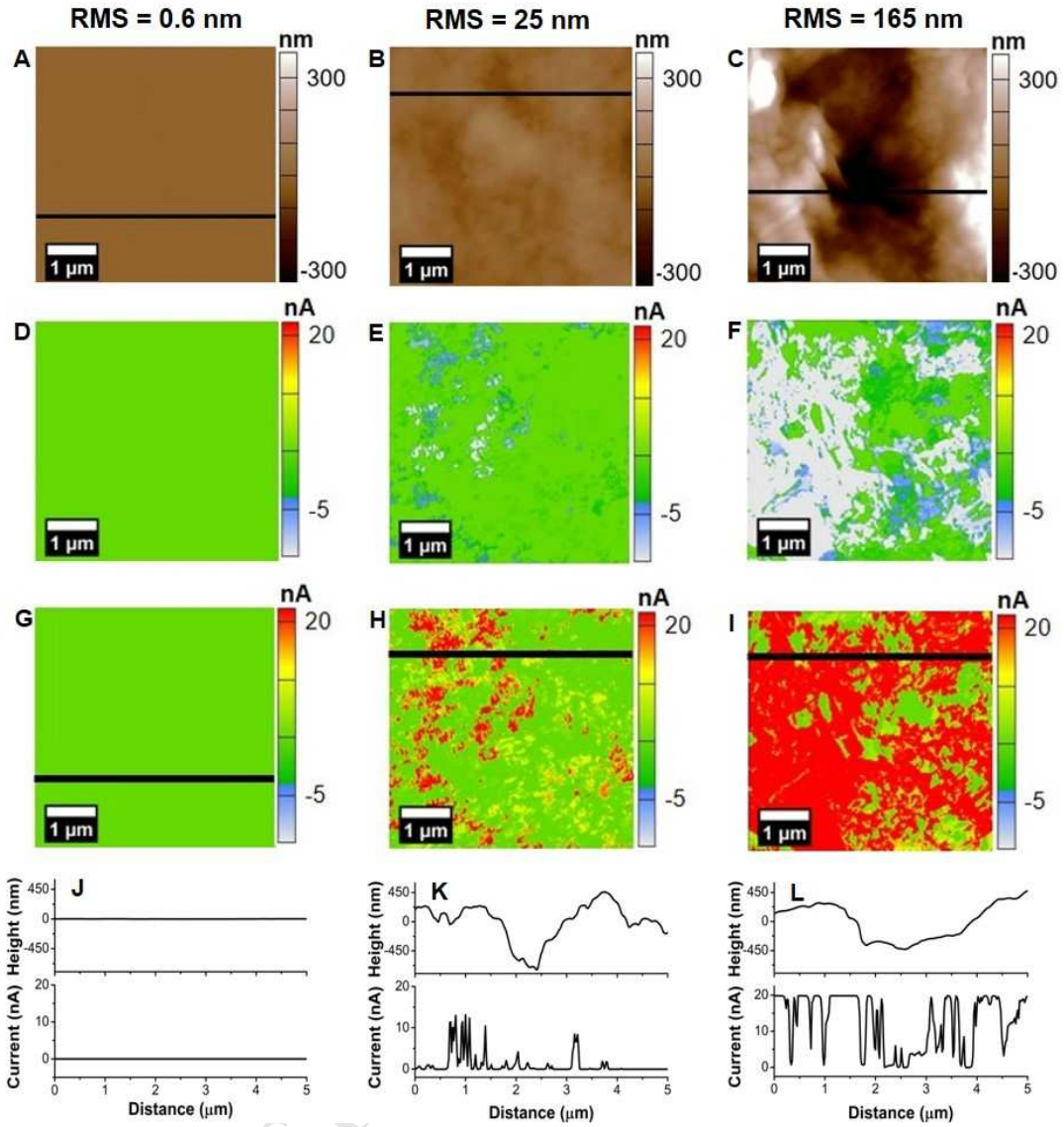

Fig. 8. Surface morphology and electrical conductivity of CS and of the bionanocomposites CS-rGO40 and CS-rGO50. AFM topographic images (5 µm x 5 µm) of (**A**) CS, (**B**) CS-rGO40 and (**C**) CS-rGO50. CAFM current images (5 µm x 5 µm) of (**D**) CS with -10V applied, (**E**) CS-rGO40 with -300 mV applied, (**F**) CS-rGO50 with -300 mV applied, (**G**) CS with 10V applied, (**H**) CS-rGO40 with 300 mV applied, (**I**) CS-rGO50 with 300 mV applied. Height and current value profiles of the marked area in the AFM and CAFM images of (**J**) CS (**K**) CS-rGO40 and (**L**) CS-rGO50.

4. Conclusions

Electrically conductive bionanocomposites were prepared considering the eco-friendly character of CS biopolymer and a non-toxic synthesis of rGO by a hydrothermal treatment of GO in the presence of a natural compound, caffeic acid, as reducing agent. To the best of authors knowledge, this work reports the CS-rGO bionanocomposites with the highest electrical conductivity and highest tensile strength achieved using a green reduction strategy. The hydrothermal reduction of GO in the presence of caffeic acid, preserved oxygen containing groups necessary to interact with CS amine groups and promote the reinforcement of the bionanocomposite materials reflected in the increase of mechanical and water resistance. Moreover, the bionanocomposite films present remarkable high antioxidant properties. The eco-friendly character of these flexible biomaterials associated with the electrical, mechanical, and antioxidant properties, make this material suitable to be used for several applications, like food packaging, body sensors and electric responsive biocompatible devices.

Acknowledgement

This work was developed within the scope of the projects: CICECO-Aveiro Institute of Materials, POCI-01-0145-FEDER-007679 (FCT Ref. UID /CTM /50011/2013); and I3N (FCT REF. UID/CTM/50025/2013) financed by national funds through the FCT/MEC and when appropriate co-financed by FEDER under the PT2020 Partnership Agreement. The project M-ERA-NET2/0021/2016 – BIOFOODPACK - Biocomposite Packaging for Active Preservation of Food is acknowledged for funding together with ECSEL-H2020 project 1/1.1.3/31.01.2018, POC-SMIS code 115833 - R3PowerUP. CN, NMF and PF

428 thank FCT for the grants (SFRH/BPD/100627/2014, SFRH/BPD/111460/2015 and
429 IF/00300/2015, respectively). This research was partially supported by COST action 15107,
430 Grants No. 101016-080937 and 38973. This publication has emanated from research
431 supported in part by a research grant from Science Foundation (SFI) under the US-Ireland
432 R&D Partnership Programme Grant Number SFI/14/US/I3113. Some of the measurements
433 were performed on equipment funded by SFI (SFI/07/IN1/B931).

434

References

[1] N. Golafshan, M. Kharaziha, M. Fathi, Tough and conductive hybrid graphene-PVA: Alginate fibrous scaffolds for engineering neural construct, Carbon N. Y. 111 (2017) 752–763. doi:10.1016/j.carbon.2016.10.042.

[2] H. Kim, H. Lee, K.Y. Seong, E. Lee, S.Y. Yang, J. Yoon, Visible Light-Triggered On-Demand Drug Release from Hybrid Hydrogels and its Application in Transdermal Patches, Adv. Healthc. Mater. 4 (2015) 2071–2077. doi:10.1002/adhm.201500323.

[3] S.R. Shin, C. Shin, A. Memic, S. Shadmehr, M. Miscuglio, H.Y. Jung, S.M. Jung, H. Bae, A. Khademhosseini, X. Tang, M.R. Dokmeci, Aligned Carbon Nanotube-Based Flexible Gel Substrates for Engineering Biohybrid Tissue Actuators, Adv. Funct. Mater. 25 (2015) 4486–4495. doi:10.1002/adfm.201501379.

[4] B. Roodenburg, S.W.H. De Haan, J.A. Ferreira, P. Coronel, P.C. Wouters, V. Hatt, Toward 6 log10 pulsed electric field inactivation with conductive plastic packaging material, J. Food Process Eng. 36 (2013) 77–86. doi:10.1111/j.1745-4530.2011.00655.x.

[5] G. Kaur, R. Adhikari, P. Cass, M. Bown, P. Gunatillake, Electrically conductive polymers and composites for biomedical applications, RSC Adv. 5 (2015) 37553–37567. doi:10.1039/c5ra01851j.

[6] U. Siripatrawan, P. Kaewklin, Fabrication and characterization of multifunctional active food packaging from chitosan-titanium dioxide nanocomposite as ethylene scavenging and antimicrobial film, Food Hydrocoll. (2018). doi:10.1016/j.foodhyd.2018.04.049.

[7] M. Motiei, S. Kashanian, L.A. Lucia, M. Khazaei, Intrinsic parameters for the synthesis and tuned properties of amphiphilic chitosan drug delivery nanocarriers, J. Control. Release. 260 (2017) 213–225. doi:10.1016/j.jconrel.2017.06.010.

[8] D.H. Ngo, S.K. Kim, Antioxidant effects of chitin, chitosan, and their derivatives, 1st ed., Elsevier Inc., 2014. doi:10.1016/B978-0-12-800268-1.00002-0.

460 [9] M. Qiu, C. Wu, G. Ren, X. Liang, X. Wang, J. Huang, Effect of chitosan and its derivatives
461 as antifungal and preservative agents on postharvest green asparagus, Food Chem. 155
462 (2014) 105–111. doi:10.1016/j.foodchem.2014.01.026.
463 [10] P. Fernandez-Saiz, J.M. Lagarón, M.J. Ocio, Optimization of the film-forming and storage
464 conditions of chitosan as an antimicrobial agent, J. Agric. Food Chem. 57 (2009) 3298–
465 3307. doi:10.1021/jf8037709.
466 [11] T. Zhou, X. Qi, H. Bai, Q. Fu, The different effect of reduced graphene oxide and graphene
467 oxide on the performance of chitosan by using homogenous fillers, RSC Adv. 6 (2016)
468 34153–34158. doi:10.1039/C6RA02225A.
469 [12] A.R. Karimi, A. Khodadadi, Mechanically Robust 3D Nanostructure Chitosan-Based
470 Hydrogels with Autonomic Self-Healing Properties, ACS Appl. Mater. Interfaces. 8 (2016)
471 27254–27263. doi:10.1021/acsami.6b10375.
472 [13] S.R. Shin, C. Zihlmann, M. Akbari, P. Assawes, L. Cheung, K. Zhang, V. Manoharan, Y.S.
473 Zhang, M. Yüksekkaya, K.T. Wan, M. Nikkhah, M.R. Dokmeci, X.S. Tang, A.
474 Khademhosseini, Reduced Graphene Oxide-GelMA Hybrid Hydrogels as Scaffolds for
475 Cardiac Tissue Engineering, Small. 12 (2016) 3677–3689. doi:10.1002/smll.201600178.
476 [14] S. Agarwal, X. Zhou, F. Ye, Q. He, G.C.K. Chen, J. Soo, F. Boey, H. Zhang, P. Chen,
477 Interfacing Live Cells with Nanocarbon Substrates, Langmuir. 26 (2010) 2244–2247.
478 doi:10.1021/la9048743.
479 [15] K. Goh, J.K. Heising, Y. Yuan, H.E. Karahan, L. Wei, S. Zhai, J.X. Koh, N.M. Htin, F.
480 Zhang, R. Wang, A.G. Fane, M. Dekker, F. Dehghani, Y. Chen, Sandwich-Architectured
481 Poly(lactic acid)-Graphene Composite Food Packaging Films, ACS Appl. Mater. Interfaces.
482 8 (2016) 9994–10004. doi:10.1021/acsami.6b02498.
483 [16] P.P. Peregrino, M.J.A. Sales, M.F.P. Da Silva, M.A.G. Soler, L.F.L. Da Silva, S.G.C.
484 Moreira, L.G. Paterno, Thermal and electrical properties of starch-graphene oxide
485 nanocomposites improved by photochemical treatment, Carbohydr. Polym. 106 (2014) 305–

311. doi:10.1016/j.carbpol.2014.02.008.

[17] H. Nassira, A. Sánchez-Ferrer, J. Adamcik, S. Handschin, H. Mahdavi, N. Taheri Qazvini, R. Mezzenga, Gelatin–Graphene Nanocomposites with Ultralow Electrical Percolation Threshold, Adv. Mater. 28 (2016) 6914–6920. doi:10.1002/adma.201601115.

[18] X. Yan, F. Li, K. Di Hu, J. Xue, X.F. Pan, T. He, L. Dong, X.Y. Wang, Y.D. Wu, Y.H. Song, W.P. Xu, Y. Lu, Nacre-mimic Reinforced Ag@reduced Graphene Oxide-Sodium Alginate Composite Film for Wound Healing, Sci. Rep. 7 (2017) 1–10. doi:10.1038/s41598-017-14191-5.

[19] D.C. Marcano, D. V. Kosynkin, J.M. Berlin, A. Sinitskii, Z. Sun, A. Slesarev, L.B. Alemany, W. Lu, J.M. Tour, Improved synthesis of graphene oxide, ACS Nano. 4 (2010) 4806–4814. doi:10.1021/nn1006368.

[20] S. Pei, H.M. Cheng, The reduction of graphene oxide, Carbon N. Y. 50 (2012) 3210–3228. doi:10.1016/j.carbon.2011.11.010.

[21] K.K.H. De Silva, H.H. Huang, R.K. Joshi, M. Yoshimura, Chemical reduction of graphene oxide using green reductants, Carbon N. Y. 119 (2017) 190–199. doi:10.1016/j.carbon.2017.04.025.

[22] M.T.H. Aunkor, I.M. Mahbubul, R. Saidur, H.S.C. Metselaar, The green reduction of graphene oxide, RSC Adv. 6 (2016) 27807–27828. doi:10.1039/C6RA03189G.

[23] T. Zhou, F. Chen, K. Liu, H. Deng, Q. Zhang, A simple and efficient method to prepare graphene by reduction of graphite oxide with sodium hydrosulfite, Nanotechnology. 22 (2011) 045704. doi:10.1088/0957-4484/22/4/045704.

[24] R. Justin, B. Chen, Body temperature reduction of graphene oxide through chitosan functionalisation and its application in drug delivery, Mater. Sci. Eng. C. 34 (2014) 50–53. doi:10.1016/j.msec.2013.10.010.

[25] J. Gao, F. Liu, Y. Liu, N. Ma, Z. Wang, X. Zhang, Environment-friendly method to produce graphene that employs vitamin C and amino acid, Chem. Mater. 22 (2010) 2213–2218.

512 doi:10.1021/cm902635j.
513 [26] Y. Wang, Z.X. Shi, J. Yin, Facile synthesis of soluble graphene via a green reduction of
514 graphene oxide in tea solution and its biocomposites, ACS Appl. Mater. Interfaces. 3 (2011)
515 1127–1133. doi:10.1021/am1012613.
516 [27] Z. Bo, X. Shuai, S. Mao, H. Yang, J. Qian, J. Chen, J. Yan, K. Cen, Green preparation of
517 reduced graphene oxide for sensing and energy storage applications., Sci. Rep. 4 (2014)
518 4684. doi:10.1038/srep04684.
519 [28] J. Zhang, H. Yang, G. Shen, P. Cheng, J. Zhang, S. Guo, Reduction of graphene oxide via L-
520 ascorbic acid., Chem. Commun. (Camb). 46 (2010) 1112–1114. doi:10.1039/b917705a.
521 [29] I. Gülçin, Antioxidant activity of caffeic acid (3,4-dihydroxycinnamic acid), Toxicology.
522 217 (2006) 213–220. doi:10.1016/j.tox.2005.09.011.
523 [30] C. Nunes, É. Maricato, Â. Cunha, A. Nunes, J. a L. da Silva, M. a Coimbra, Chitosan-caffeic
524 acid-genipin films presenting enhanced antioxidant activity and stability in acidic media.,
525 Carbohydr. Polym. 91 (2013) 236–43. doi:10.1016/j.carbpol.2012.08.033.
526 [31] Y.-K. Kim, M.-H. Kim, D.-H. Min, Biocompatible reduced graphene oxide prepared by
527 using dextran as a multifunctional reducing agent, Chem. Commun. 47 (2011) 3195.
528 doi:10.1039/c0cc05005a.
529 [32] W. Lv, C. Zhang, Z. Li, Q.H. Yang, Self-assembled 3D graphene monolith from solution, J.
530 Phys. Chem. Lett. 6 (2015) 658–668. doi:10.1021/jz502655m.
531 [33] K. Hu, X. Xie, T. Szkopek, M. Cerruti, Understanding Hydrothermally Reduced Graphene
532 Oxide Hydrogels: From Reaction Products to Hydrogel Properties, Chem. Mater. 28 (2016)
533 1756–1768. doi:10.1021/acs.chemmater.5b04713.
534 [34] R.K. Hiremath, M.K. Rabinal, B.G. Mulimani, Simple setup to measure electrical properties
535 of polymeric films, Rev. Sci. Instrum. 77 (2006) 1–4. doi:10.1063/1.2403937.
536 [35] R. Re, N. Pellegrini, A. Proteggente, A. Pannala, M. Yang, C. Rice-Evans, Antioxidant
537 activity applying an improved ABTS radical cation decolorization assay, Free Radic. Biol.

538 Med. 26 (1999) 1231–1237. doi:10.1016/S0891-5849(98)00315-3.
539 [36] Z. Su, H. Wang, K. Tian, F. Xu, W. Huang, X. Tian, Simultaneous reduction and surface
540 functionalization of graphene oxide with wrinkled structure by diethylenetriamine (DETA)
541 and their reinforcing effects in the flexible poly(2-ethylhexyl acrylate) (P2EHA) films,
542 Compos. Part A Appl. Sci. Manuf. 84 (2016) 64–75.
543 doi:10.1016/j.compositesa.2015.11.033.
544 [37] H. Feng, R. Cheng, X. Zhao, X. Duan, J. Li, A low-temperature method to produce highly
545 reduced graphene oxide, Nat. Commun. 4 (2013) 1537–1539. doi:10.1038/ncomms2555.
546 [38] M.T.H. Aunkor, I.M. Mahbubul, R. Saidur, H.S.C. Metselaar, The green reduction of
547 graphene oxide, RSC Adv. 6 (2016) 27807–27828. doi:10.1039/C6RA03189G.
548 [39] N. Cartier, A. Domard, H. Chanzy, Single crystals of chitosan, Int. J. Biol. Macromol. 12
549 (1990) 289–294. doi:10.1016/0141-8130(90)90015-3.
550 [40] D. Long, W. Li, L. Ling, J. Miyawaki, I. Mochida, S.H. Yoon, Preparation of nitrogen-
551 doped graphene sheets by a combined chemical and hydrothermal reduction of graphene
552 oxide, Langmuir. 26 (2010) 16096–16102. doi:10.1021/la102425a.
553 [41] J.-B. Wu, M.-L. Lin, X. Cong, H.-N. Liu, P.-H. Tan, Raman spectroscopy of graphene-based
554 materials and its applications in related devices, Chem. Soc. Rev. (2018) 1822–1873.
555 doi:10.1039/C6CS00915H.
556 [42] S. Stankovich, D.A. Dikin, R.D. Piner, K.A. Kohlhaas, A. Kleinhammes, Y. Jia, Y. Wu,
557 S.B.T. Nguyen, R.S. Ruoff, Synthesis of graphene-based nanosheets via chemical reduction
558 of exfoliated graphite oxide, Carbon N. Y. 45 (2007) 1558–1565.
559 doi:10.1016/j.carbon.2007.02.034.
560 [43] A.C. Ferrari, D.M. Basko, Raman spectroscopy as a versatile tool for studying the properties
561 of graphene, Nat. Nanotechnol. 8 (2013) 235–246. doi:10.1038/nnano.2013.46.
562 [44] N. Díez, A. Śliwak, S. Gryglewicz, B. Grzyb, G. Gryglewicz, Enhanced reduction of
563 graphene oxide by high-pressure hydrothermal treatment, RSC Adv. 5 (2015) 81831–81837.

564 doi:10.1039/C5RA14461B.

565 [45] J.-L. Shi, W.-C. Du, Y.-X. Yin, Y.-G. Guo, L.-J. Wan, Hydrothermal reduction of three-
566 dimensional graphene oxide for binder-free flexible supercapacitors, J. Mater. Chem. A. 2
567 (2014) 10830. doi:10.1039/c4ta01547a.

568 [46] R. Priyadarshi, B. Kumar, Y.S. Negi, Chitosan film incorporated with citric acid and
569 glycerol as an active packaging material for extension of green chilli shelf life, Carbohydr.
570 Polym. 195 (2018) 329–338. doi:10.1016/j.carbpol.2018.04.089.

571 [47] A.S. Ferreira, C. Nunes, A. Castro, P. Ferreira, M. a. Coimbra, Influence of grape pomace
572 extract incorporation on chitosan films properties, Carbohydr. Polym. 113 (2014) 490–499.
573 doi:10.1016/j.carbpol.2014.07.032.

574 [48] S. Prateepchanachai, W. Thakhiew, S. Devahastin, Mechanical properties improvement of
575 chitosan films via the use of plasticizer , charge modifying agent and film solution
576 homogenization, Carbohydr. Polym. 174 (2017) 253–261.
577 doi:10.1016/j.carbpol.2017.06.069.

578 [49] M. Zappino, I. Cacciotti, I. Benucci, F. Nanni, K. Liburdi, F. Valentini, M. Esti, Bromelain
579 immobilization on microbial and animal source chitosan fi lms , plasticized with glycerol ,
580 for application in wine-like medium : Microstructural , mechanical and catalytic
581 characterisations, Food Hydrocoll. 45 (2015) 41–47. doi:10.1016/j.foodhyd.2014.11.001.

582 [50] R. Justin, B. Chen, Strong and conductive chitosan-reduced graphene oxide nanocomposites
583 for transdermal drug delivery, J. Mater. Chem. B. 2 (2014) 3759–3770.
584 doi:10.1039/c4tb00390j.

585 [51] S.K. Yadav, Y.C. Jung, J.H. Kim, Y. Il Ko, H.J. Ryu, M.K. Yadav, Y.A. Kim, J.W. Cho,
586 Mechanically robust, electrically conductive biocomposite films using antimicrobial
587 chitosan-functionalized graphenes, Part. Part. Syst. Charact. 30 (2013) 721–727.
588 doi:10.1002/ppsc.201300044.

589 [52] X. Wang, H. Bai, Z. Yao, A. Liu, G. Shi, Electrically conductive and mechanically strong

biomimetic chitosan/reduced graphene oxide composite films, J. Mater. Chem. 20 (2010) 9032. doi:10.1039/c0jm01852j.

[53] I. Gonç Alves, C. Nunes, S. Mendes, L.O. Martins, P. Ferreira, M.A. Coimbra, CotA laccase-ABTS/hydrogen peroxide system: An efficient approach to produce active and decolorized chitosan-genipin films, Carbohydr. Polym. 175 (2017) 628–635. doi:10.1016/j.carbpol.2017.08.029.

[54] Y. Luo, X. Pan, Y. Ling, Facile fabrication of chitosan active film with xylan via direct immersion, Cellulose. 21 (2014) 1873–1883. doi:10.1007/s10570-013-0156-4.

[55] J.-R. Ye, L. Chen, Q. Zhang, Q. Shen, Turning the chitosan surface from hydrophilic to hydrophobic by layer-by-layer electro-assembly, RSC Adv. 4 (2014) 58200. doi:10.1039/C4RA10327K.

[56] B.D. De Britto, O.B.G. Assis, Hydrophilic and Morphological Aspects of Films Based on Quaternary Salts of Chitosan for Edible Applications, Packag. Technol. Sci. 23 (2010) 111–119. doi:10.1002/pts.

[57] L.J. Cote, R. Cruz-Silva, J. Huang, Flash Reduction and Patterning of Graphite Oxide and Its Polymer Composite, J. Am. Chem. Soc. 131 (2009) 11027–11032.

[58] M. Abolhassani, C.S. Griggs, L.A. Gurtowski, J.A. Mattei-Sosa, M. Nevins, V.F. Medina, T.A. Morgan, L.F. Greenlee, Scalable Chitosan-Graphene Oxide Membranes: The Effect of GO Size on Properties and Cross-Flow Filtration Performance, ACS Omega. 2 (2017) 8751–8759. doi:10.1021/acsomega.7b01266.

[59] K. Kosowska, P. Domalik-pyzik, M. Nocu, J. Ch, Chitosan and graphene oxide / reduced graphene oxide hybrid nanocomposites – Evaluation of physicochemical properties, Mater. Chem. Phys. 216 (2018) 28–36. doi:10.1016/j.matchemphys.2018.05.076.

[60] Y. Qiu, Z. Wang, A.C.E. Owens, I. Kulaots, Y. Chen, A.B. Kane, R.H. Hurt, Antioxidant chemistry of graphene-based materials and its role in oxidation protection technology, Nanoscale. 6 (2014) 11744–11755. doi:10.1039/c4nr03275f.

[61] N. Yousefi, M.M. Gudarzi, Q. Zheng, S.H. Aboutalebi, F. Sharif, J.-K. Kim, Self-alignment and high electrical conductivity of ultralarge graphene oxide–polyurethane nanocomposites, J. Mater. Chem. 22 (2012) 12709. doi:10.1039/c2jm30590a.

[62] S. Wan, J. Peng, Y. Li, H. Hu, L. Jiang, Q. Cheng, Use of Synergistic Interactions to Fabricate Strong, Tough, and Conductive Artificial Nacre Based on Graphene Oxide and Chitosan, ACS Nano. 9 (2015) 9830–9836. doi:10.1021/acsnano.5b02902.